Grid Inertia Estimation Using Inverter-Based Resource Power Plant Data

Huazhao Ding, Rabi Kar, Zhixin Miao, Lingling Fan
University of South Florida, Tampa, FL 33620, USA
Email: {huazhao, rskar, zmiao, linglingfan}@usf.edu

***Abstract*—This paper proposes a method for estimating key grid dynamic parameters, such as inertia and damping, of a power grid using an inverter-based resource (IBR) power plant's data stream collected at its point of interconnection. The effect of grid strength on measurements, more specifically, frequency responses, is first investigated to clarify the application scope, a detail often overlooked in previous studies. Based on the collected real power and frequency measurements, the grid model structures are proposed and the model parameters (such as inertia, damping, droop parameters) are estimated using system identification methods. The estimation approach is demonstrated using an electromagnetic transient simulation testbed, developed in MATLAB/Simscape for data generation. Model parameter estimation is further carried out using the collected data.**

***Index Terms*—Grid inertia estimation, synchronous generator, inverter-based resource, grid strength, system identification.**

I. Introduction

Inertia is an important parameter to monitor in power grids since this parameter directly influences the grid's frequency response. In ERCOT, online inertia is computed by aggregating all online generator's inertia [1]. Additionally, inertia can be estimated using event data after MW loss. For example, [1] has analyzed 137 real-world MW loss events in Texas during 2010. Based on the MW loss information and the rate of frequency change, inertia can be estimated to be within the 10% error range. ERCOT's inertia in 2010 was in the range of 300 to 500 MW/0.1 Hz. This approach is termed as disturbance-based method in [2].

The disturbance-based methods are among the earliest and most intuitive, relying on fitting the swing equation to post-disturbance frequency and power trajectories. Similar to the inertia estimation method mentioned in [1], approaches in [3], [4] use immediate frequency deviations following generation or load changes to estimate system inertia. In [3], inertia is computed by detecting a disturbance and using two sets of power measurements and rate of frequency change values. In [4], both the effects of governor control and voltage on frequency responses are taken into consideration to estimate inertia. The method is tested and validated using Nordic 57-bus test system.

Besides disturbance-based methods, there are two other methods: ambiant measurement-based and probing signal-based [2]. The ambient-measurement techniques avoid waiting for large events by exploiting stochastic load/generation variability. The method uses the measured voltage and current, solves a covariance matrix using optimization and fits the result with the classical generator mathematical model to validate the result [5]. The ambient estimation process requires phasor measurement unit (PMU) data to estimate the inertia and damping.

A third class injects small probing signals (e.g., from an external device) to excite low-frequency dynamics safely, then estimates inertia from the measured frequency/power response. Practical demonstrations and parameterization guidance for safe probing on real networks have recently been reported [6]. Estimation methodology wise, many of the probing methods adopt the similar method of finding inertia, as the disturbance-based methods.

Goals: The goal of this paper is to rely on an inverter-based resource (IBR) power plant's measurements and estimate grid inertia. This method is in the category of injecting probing signals. There is a strong justification for this approach. First, IBR power plants are required to have PMUs installed for monitoring according to the recent NERC standards, e.g., PRC-028 [7], PRC-030 [8]. This requirement ensures that IBR power plants can provide data streams of real power and frequency. Second, an IBR power plant of solar or wind is an intermittent source and its power output is known to be fluctuant. Therefore, an IBR power plant naturally serves as the source of probing. Finally, many legacy IBR power plants do not provide frequency or inertia support, making them decoupled from frequency response. Therefore, it is ideal to use an IBR power plant's power injection as the probing signal and use the frequency measurement to estimate grid inertia.

Our contributions: In this paper, we investigate the feasibility or application scope of using IBR power plant's real power injection and frequency measurement for grid inertia estimation. We also demonstrate the system identification-based method for inertia estimation. This approach is different compared to those in [3], [4], [6]. Our approach takes full advantage of the input and output data and estimate a dynamic model and its parameters, including inertia, damping, droop parameters, etc.

The remainder of the paper is organized as follows. Section II introduces the proof of concept. Section III presents a realistic testbed and the estimation method. This section examines the effect of grid strength on frequency response. In addition, the grid information estimation process are discussed. Section IV concludes with remarks on application in practice and future extension.

979-8-3315-8138-1

II. Proof of concept

A. General concept explained

In this section, the general concept of grid inertia estimation is discussed. The process can be viewed as two parts: data generation and estimation. To have a better view of the process, we first need to understand how real power and frequency are associated with inertia and damping

For a synchronous generator serving a load, the inertia and damping of the machine are two key parameters of the swing dynamics, , which is shown as swing Eq. 1.

$$2H\frac{d\omega}{dt} + D\omega = P_m - P_e, \tag{1}$$

where P_m is the mechanical power in pu, P_e is the electric power in pu, ω is the rotating speed in pu, H is the inertia in the unit of pu.s/pu and D is the damping coefficient in pu.

The system's frequency and the synchronous generator's rotating speed are the same thing. It can be seen that the input/output relationship between the frequency and the power is as follows.

$$\frac{\Delta\omega}{\Delta P} = \frac{1}{2Hs + D}. \tag{2}$$

During an event, the deviation of the input and output can be measured and processed through data acquisition. Based on the input and output time-series data, the transfer function can be identified through system identification method. In MATLAB, *tfest* function can be used to process the input and output data, while outputting a transfer function of desired order.

To explain this concept, a simple testbed is built in Fig. 1, where a 2-MVA synchronous generator serves a load. Constant mechanical power is assumed and the generator serves four parallel connected loads (Load 1-4) was built, as shown in Fig. 1. The inertia and damping of the synchronous machine are known as $H = 0.6$ and $D = 10$. These two parameters are not for a realistic generator. Rather, they have been tuned to provide a fast and well damped inertia response. Parallel connected loads were switched using circuit breakers (B1-B3) at regular intervals. B1 is initially opened, while B2 and B3 are closed. The total system load is 1.6 MW or 0.8 pu. Then, B1 is switched on at 2 s, B3 is switched off at 4 s, and B2 is switched off at 6 s, respectively, to create the system events. At $t = 2$ s, the total load is 2.4 MW or 1.2 pu. At $t = 4$ s, the total load reduces to 2.1 MW. At $t = 6$ s, the total load reduces to 1.7 MW. The meter is located at the terminal of the synchronous generator and measures P and ω.

Input (real power deviation) and the output (frequency deviation) data are presented in Fig. 2.

A first-order transfer function is estimated using *tfest* based on the input and output data. The model's output for the same input is shown in Fig. 2, subplot 3. Identification uses the first power step beginning at 2 seconds. The window selected for *tfest* is from 1.9 seconds to 3.5 seconds, which covers a whole dynamic from the pre-event to post-event steady state. The identified transfer function is given in Eq. (3). This transfer function's output matches the measurement data at a matching degree close to 100%. By equating Eq. (2) with Eq. (3) and

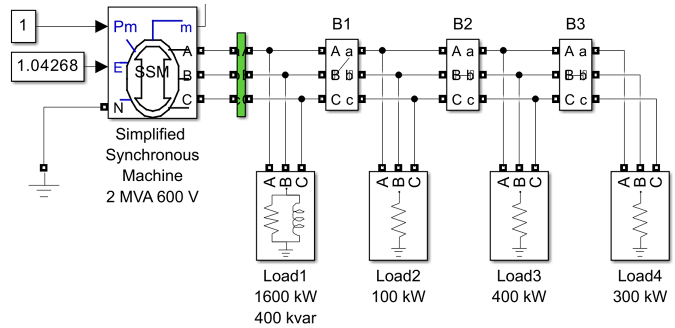

Fig. 1: A simplified synchronous machine system with loads. The machine's power and voltage based are 2 MVA and 600 V, respectively. Four constant power loads will consume 0.8 pu, 0.05 pu, 0.2 pu, and 0.15 pu real power, respectively.

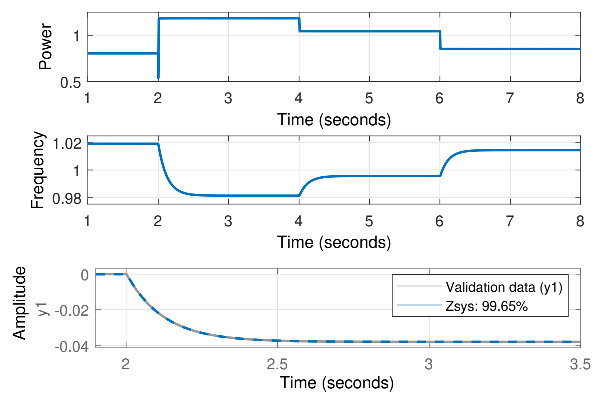

Fig. 2: Subplot 1): input power; subplot 2): output frequency; subplot 3) *tfest* estimation with measured power and frequency..

matching coefficients, the estimated parameters are $H = 0.607$ and $D = 9.99$, which are consistent with the settings of the synchronous machine.

$$\frac{\Delta\omega}{\Delta P} = \frac{0.8241}{1s + 8.23} = \frac{1}{12.134s + 9.9867}. \tag{3}$$

The above method proves that grid information, such as inertia and damping, can be estimated using a measurement-based method with transfer function estimation. In addition to the load switch, data can be generated using real power injection from an IBR power plant.

III. Estimation based on data of IBR power plant

An IBR power plant, which operates in grid-following control mode, is connected to the external power grid. The grid itself can be represented by different models, ranging from a classical synchronous machine equivalent to reduced-order network representations. By applying a small controlled real power change on the IBR side and recording the local P and f responses at the IBR side measurement location, one can infer key dynamic parameters of the surrounding grid.

On the other hand, there is a key question to be addressed before this method is applicable: Whether the frequency measurement at the IBR power plant really align with the

979-8-3315-8138-1

frequency measurement of the grid? To address this question, a testbed of IBR grid integration is built. The effect of grid strength on measurement data is also examined.

A. Testbed

To study how location of measurement and grid strength affect estimation, we developed a more detailed benchmark system. The general configuration of the system is shown in Fig. 3. The network consists of two main areas: Area 1: grid, which contains conventional synchronous generation, and Area 2: IBR, which include a transformer and transmission corridor.

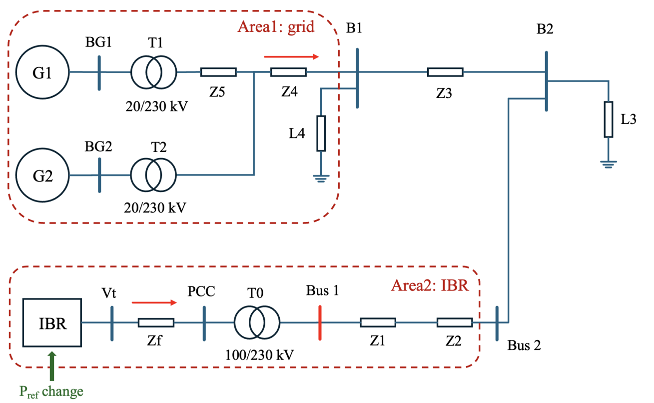

Fig. 3: Structure of the system. G1: 900 MVA. G2: 900 MVA. IBR: 200 MVA.

In general, the system in Fig. 3 can be divided into three voltage zones defined by the transformer ratings: 1. The IBR zone at 100 kV; 2. The transmission zone at 230 kV; 3. The synchronous generation zone at 20 kV. The transmission and synchronous generation portions of this testbed are adapted from the classic Kundur two-area benchmark system [9] implemented in MATLAB/SimScape. In this configuration, Area 2 of the original model is replaced with the grid-following IBR subsystem. The generators are equipped with excitation control and speed-governor control.

The IBR subsystem operates at 100 kV and is connected at bus PCC through a transformer T0 (100/230 kV). The inverter terminal is represented by V_t, and a filter impedance Z_f is included between the inverter and the PCC bus. The IBR adopts a cascaded structure with an outer power control loop (real and reactive power regulation) and an inner current control loop, coordinated by a phase-locked loop (PLL) for synchronization.

B. Data acquisition: grid strength test

To collect data for estimation, a step change in the real power reference was applied to the IBR's real power control, where the output was reduced from 1.0 pu to 0.55 pu at $t = 160$ s. In terms of the 230-kV side of transformer T0 (900 MVA), this corresponds to a reduction from 0.22 pu to 0.12 pu. The frequency and power responses were monitored at multiple buses across the system, including the PCC, bus 1, B1, BG1, and BG2. To capture the influence of grid strength, both strong-grid and weak-grid operating conditions were considered, as the system dynamics are expected to differ between the two cases. The resulting time-domain frequency responses are presented in Fig. 4.

At steady state, the step reduction in the IBR power reference directly affects the overall power balance on the grid side. Since both SGs and IBR supply the power that is ultimately consumed by constant power loads, a decrease in IBR output is similar to an increase in loads. Therefore, the synchronous generator's speed will reduce and stabilize to a lower value. This helps the speed-governor control of the generator to increase the mechanical power, thereby balancing the loss of generation from the IBR.

A comparison between the weak and strong grid strength is shown in Fig. 4a and Fig. 4b. In the weak grid case Fig. 4a, the IBR-side frequency trajectory generally follows the SG-side frequency after the reference change, but important differences appear, particularly in the initial undershoot of the IBR frequency, which deviates significantly from the SG and bus B1 responses. On the other hand, for the strong grid strength Fig. 4b, the IBR and the grid's frequency responses are more alike. Since SG frequency and power responses directly reflect the inertia and damping characteristics of the grid system, these discrepancies, between the IBR side frequency responses and the SG side, introduce potential bias and reduce the accuracy of the estimate under weak grid conditions. For this reason, the strong-grid case can be adopted for parameter estimation.

Remark 1: We base our estimation on the strong-grid case because it preserves the key assumption that bus frequencies are coherent (or nearly identical) across the system.

C. Grid inertia estimation

The input/output data from theIBR are shown in Fig. 5. The signals are acquired from Bus 1 (labeled in Fig. 3). Following a step change in the IBR power reference, the frequency response takes approximately 80 seconds to reach steady state. Since the synchronous generators in Area 1 have a more complex control, the dynamic response of the measured frequency shows that the system cannot be simply identified by a first-order *tfest*. Therefore, the selection of the model order for the *tfest* and the design of the higher-order system structure for mapping are necessary.

1) 2nd order model: Since the *tfest* method needs to configure the window size and the system order, the estimated transfer function will also perform a different mapping rate depending on the configuration. The idea situation is to use the lowest order and shorter window size to achieve an accurate estimation. Based on this principle, multiple tests are executed.

Fig. 6 shows the estimation with different window sizes when the desired transfer function is a second-order system. It can be seen that when the window length is selected as 10 seconds after the event, a second-order system can be used to describe the output frequency well. However, the total dynamic lasts at least 80 seconds after the IBR side event. The third subplot shows the dynamic response comparison for 60

979-8-3315-8138-1

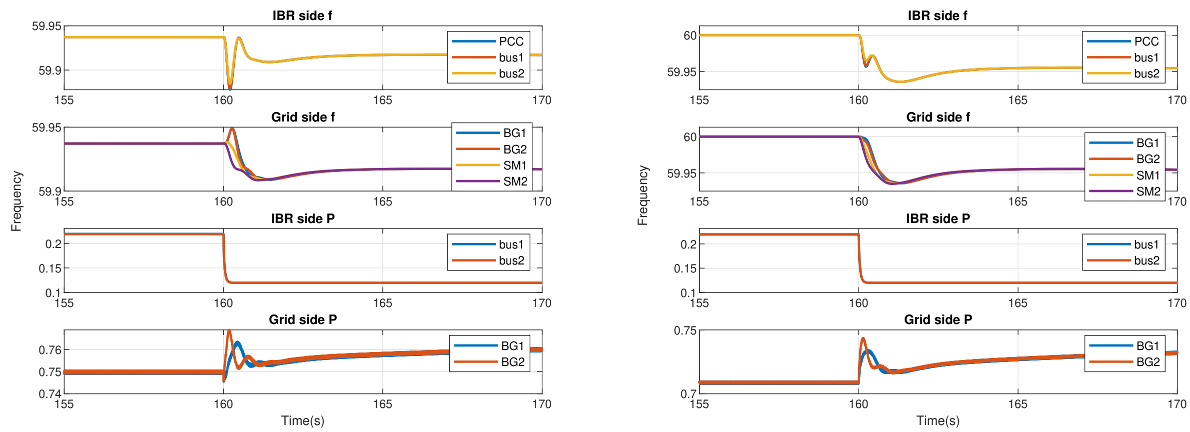

(a) Weak grid condition.

(b) Strong grid condition.

Fig. 4: Frequency and power response after IBR side power step change (a) Weak grid (SCR = 3.4). (b) Strong grid (SCR = 8.3).

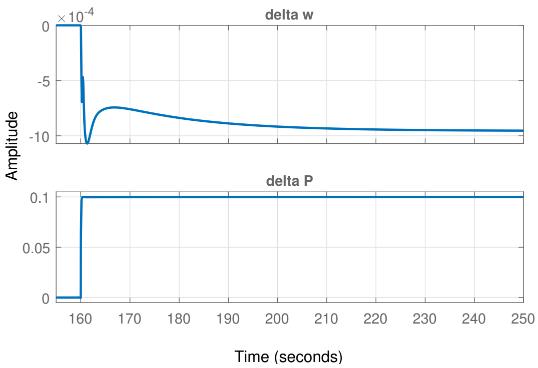

Fig. 5: IBR area bus 1 strong grid input output.

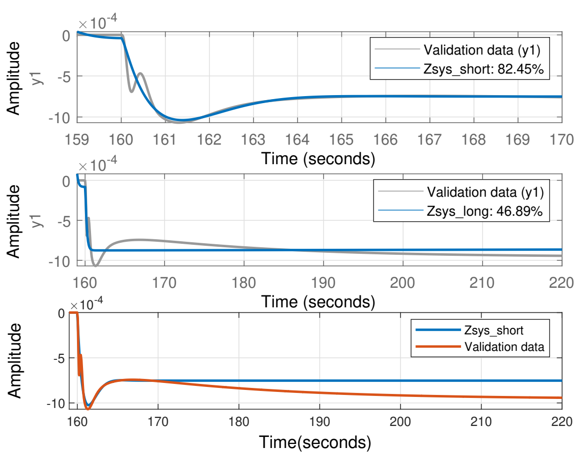

Fig. 6: Second-order transfer function estimation with different window size selecting. subplot 1): estimation with short window size data, subplot 2): estimation with long window size, subplot 3): comparison between frequency response of short window size estimated system and simulation results.

seconds. It can be seen that this second-order system cannot provide accurate steady-state response.

The second subplot of Fig. 6 shows the second-order estimation with a larger window size. This model cannot accurately reflect the first 10 seconds' dynamics.

The second-order representation is not sufficient to capture the steady-state relationship of frequency vs. power, which is most associated with H and the droop parameter R.

The model structure is shown in Fig. 7, where not only the swing dynamics but also the speed governor control has been included.

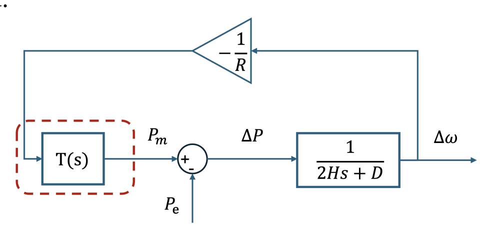

Fig. 7: Model structure.

For the second-order case, $T(s)$ may be assumed as $1/(as+1)$, which represents the mechanical power versus the power order relationship. The closed-loop transfer function and data estimated transfer function are shown as Eq. (4) and Eq. (5), respectively.

$$\frac{\Delta\omega_{2^{nd}}}{\Delta P_{2^{nd}}} = -\frac{as+1}{2aHs^2+(2H+aD)s+D+\frac{1}{R}}. \tag{4}$$

$$G(s)_{2^{nd}} = -\frac{1.69s+1}{81.7s^2+166.6s+132.8}. \tag{5}$$

By mapping Eq. (4) and Eq. (5), we can find that the estimated grid inertia is 24.17, while the total grid inertia applied in SGs is 13 based on the power base of 900 MW.

D. 3rd order system

Further studies have been conducted by assuming the transfer function is 3rd order and a 95-s data window size is used. Fig. 8 shows the *tfest* estimate's output versus the data.

The *tfest* estimated transfer function is presented in Eq. (6).

$$G(s)_{3^{rd}} = -\frac{0.02389s^2+0.008987s+0.0005723}{1s^3+2.253s^2+1.289s+0.05962}. \tag{6}$$

979-8-3315-8138-1

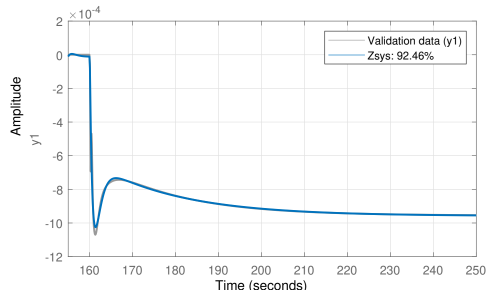

Fig. 8: Third-order transfer function estimation.

TABLE I: Estimated parameters across tests.

	gen parameters	Test 1	Test 2	Test 3	Test 4
System order	N/A	2	2	3 (Type I)	3 (Type II)
Window length (s)	N/A	10	30	90	90
H	13	24.17	27.27	35.5	21
D	0	80.2	69.99	70.21	80
$\frac{1}{R}$	80	62.85	71.75	33.96	24.6

$T(s)$ is assumed to be a 2nd-order system with two representations: $1/(as^2+bs+1)$ or $(ds+1)/(as^2+bs+1)$. The corresponding derived transfer functions are presented in Eq. (7) and Eq. (8).

$$\frac{\Delta\omega_{3^{rd},I}}{\Delta P_{3^{rd},I}} = -\frac{as^2+bs+1}{2aHs^3+(2bH+aD)s^2+\left(bD+2H\right)s+D+\frac{1}{R}}. \quad (7)$$

$$\frac{\Delta\omega_{3^{rd},II}}{\Delta P_{3^{rd},II}} = -\frac{as^2+bs+1}{2aHs^3+(2bH+aD)s^2+\left(bD+2H+\frac{d}{R}\right)s+D+\frac{1}{R}}. \quad (8)$$

The grid inertia can be found by mapping the derived transfer function Eq. (7) and Eq. (8) with the *tfest* estimated transfer function Eq. (6). It can be seen from Eq. (7) that there are five unknown variables: H, D, $1/R$, a and b, while the mapping between Eq. (7) and Eq. (6) can provide 6 equations. The mapping for Type I structure is conducted by nonlinear least square estimation *lsqnonlin* command. The Type II structure is performed directly by finding six unknowns (H, D, $1/R$, a, b and d) from six equations.

The estimated results with different input/output data and estimation consideration are provided in Table I. The total inertia of the two generators is 13 based on 900 MW power base. It can be seen Test 4 (3rd order assumption, 90 s data-based estimation) leads to the closest H estimation. Additionally, it can be seen that both Test 3 and Test 4 lead to the same steady-state gain of $1/(D+1/R)$.

Fig. 9 shows the Bode diagrams of the estimated transfer function in (8), the closed-loop feedback system based on parameterized model in Fig. 7, and the first-order approximation. It can be seen that the estimated parameters indeed lead to the same frequency response.

While a grid-following IBR is generally considered not contributing frequency regulation, research has found that PLL indeed contributes equivalent inertia [10]. This effect makes the measured H appears greater than the generators' total inertia. Furthermore, the EMT simulation results also show that the frequency sensor introduces delay, which again makes

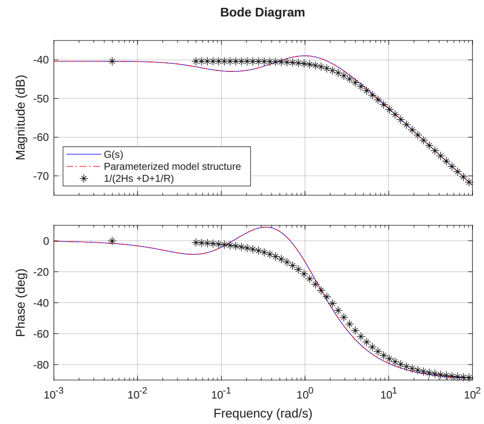

Fig. 9: Frequency response of $-\frac{\Delta\omega}{\Delta P}$.

H appear greater. Further investigation is necessary to mitigate the effect of the PLL and the frequency sensor.

IV. Conclusion and Future Work

This paper presents a method of estimating grid inertia using data taken at an IBR power plant. The investigation shows that this method is applicable when the grid is strong and the frequency response upon IBR power perturbation can lead to reasonable estimation of inertia. Furthermore, the synchronizing dynamics of the IBR may influence the estimated inertia results. Future work will focus on investigating the effect of grid condition and IBR's own synchronizing dynamics on grid inertia estimation.

References

[1] S. Sharma, S.-H. Huang, and N. Sarma, "System inertial frequency response estimation and impact of renewable resources in ercot interconnection," in *2011 IEEE Power and Energy Society General Meeting*, 2011, pp. 1–6.

[2] B. Tan, J. Zhao, M. Netto, V. Krishnan, V. Terzija, and Y. Zhang, "Power system inertia estimation: Review of methods and the impacts of converter-interfaced generations," *International Journal of Electrical Power & Energy Systems*, vol. 134, p. 107362, 2022. [Online]. Available: https://www.sciencedirect.com/science/article/pii/S0142061521006013

[3] P. Wall and V. Terzija, "Simultaneous estimation of the time of disturbance and inertia in power systems," *IEEE Transactions on Power Delivery*, vol. 29, no. 4, pp. 2018–2031, 2014.

[4] D. Zografos, M. Ghandhari, and R. Eriksson, "Power system inertia estimation: Utilization of frequency and voltage response after a disturbance," *Electric Power Systems Research*, vol. 161, pp. 52–60, 2018. [Online]. Available: https://www.sciencedirect.com/science/article/pii/S037877961830107X

[5] F. Bizzarri, D. d. Giudice, S. Grillo, D. Linaro, A. Brambilla, and F. Milano, "Inertia estimation through covariance matrix," *IEEE Transactions on Power Systems*, vol. 39, no. 1, pp. 947–956, 2024.

[6] Y. Zhao and Y. Liu, "Real-time inertia estimation using probing method and pmu measurement," *Energy Systems*, pp. 1–21, 2025.

[7] NERC, "PRC-028-1 – Disturbance Monitoring and Reporting Requirements for Inverter-Based Resources," 2023.

[8] ——, "PRC-030-1 – Unexpected Inverter-Based Resource Event Mitigation," 2024.

[9] P. Kundur, N. Balu, and M. Lauby, *Power System Stability and Control*, ser. EPRI power system engineering series. McGraw-Hill Education, 1994. [Online]. Available: https://books.google.com/books?id=wOlSAAAAMAAJ

[10] X. He, H. Geng, R. Li, and B. C. Pal, "Transient stability analysis and enhancement of renewable energy conversion system during lvrt," *IEEE Transactions on Sustainable Energy*, vol. 11, no. 3, pp. 1612–1623, 2020.

979-8-3315-8138-1